Detuned secondary instabilities in three-dimensional boundary-layer flow

Antoine Jouin,[1,2] Nicola Ciola,[1,2] Stefania Cherubini,[1] and Jean Christophe Robinet[2,*]
[1]*Dipartimento di Meccanica, Matematica e Management, Politecnico di Bari, Via Re David 200, 70125 Bari, Italy*
[2]*Laboratoire DynFluid, Arts et Métiers Institute of Technology, 151 Bd de l'Hopital, 75013 Paris, France*

(Received 24 June 2023; accepted 29 February 2024; published 2 April 2024)

In this work we apply a formulation for capturing detuned secondary instabilities. This formulation, based on two-dimensional stability analysis coupled with a Bloch wave formalism originally described by Schmidt *et al.* [Phys. Rev. Fluids **2**, 113902 (2017)], allows us to consider high-dimensional systems resulting from several repetitions of a spatially periodic unit by solving an eigenproblem of much smaller size. Secondary instabilities coupling multiple periodic units thus can be retrieved. The method is applied on the secondary stability of a swept boundary-layer flow subject to stationary cross-flow vortices. Two distinct detuned secondary instabilities are retrieved. The first one, obtained for a detuning factor $\epsilon = 0.35$ and reaching a maximum growth rate for streamwise wave number $\alpha_v = 0.087$, was already found in the work of Fischer and Dallmann [Phys. Fluids A: Fluid Dyn. **3**, 2378 (1991)]. The second instability is obtained for streamwise independent modes and small detuning factor $\epsilon = 0.08$. The corresponding mode presents large-wavelength oscillations, arising from a characteristic beating phenomenon. The physical origin of these two secondary instabilities has been investigated by varying the amplitude of the primary disturbance: for the latter instability, reminiscent of a type III mode, the unstable branch continuously deforms as the amplitude is increased, whereas a change of topology of the spectrum is observed for the $\alpha_v = 0$ mode.

DOI: 10.1103/PhysRevFluids.9.043901

I. INTRODUCTION

Transition to turbulence is a crucial problem of great technical interest in fluid mechanics. A successful approach for studying it consists in dividing the process into several stages. An initial stage, denoted as primary instability, can be investigated through linear stability theory, either modal or nonmodal [1]. These analyses yield structures representative of the primary instability mechanisms such as Tollmien-Schlichting (TS) waves for channel or boundary-layer flows [2], cross-flow vortices for swept flows [3], gravity waves in stratified flows [4], or streaks in the case of nonmodal mechanisms [5]. This list is far from being exhaustive as the relevant structures strongly depend on the flow configuration and the case considered.

These flow structures are likely to further destabilize, resulting in the second stage of the transition process. Investigation of this stage is possible through secondary stability theory, established through the seminal works of Orszag and Patera [6] and Herbert [7] on two-dimensional TS waves in wall-bounded flows. In the simplest cases, secondary stability theory is based on a Floquet analysis of a secondary base flow constructed as the superposition of an initial laminar flow and a primary disturbance previously identified. In channel and boundary layer flows, the exponential growth of small three-dimensional disturbances, observed experimentally and in numerical simulations, was

*jean-christophe.robinet@ensam.eu

explained as a secondary instability of two-dimensional TS waves [6,7]. Following these seminal works, the theory was applied to numerous other configurations such as streaks in boundary-layer [8] or cross-flow vortices in swept flows [9,10], leading to breakthroughs in the identification of the underlying mechanisms of transition to turbulence.

Peculiar long-wavelength modes can be observed in several flow configurations, usually coupling multiple length scales, such as the flow over superhydrophobic surfaces with moving interfaces [11], large arrays of vortices [12], or vortex pairings in mixing layers [13]. The origin of such long-wavelength, detuned modes can be investigated by means of secondary instability of primary modes. In this article we introduce a formulation for secondary stability analysis based on the association of a local two-dimensional stability analysis and a Bloch wave formalism. This formulation is based on the mathematical framework proposed by Schmid *et al.* [14] for the primary stability analysis of fluid systems consisting of a spatially periodic array of n identical units. A similar framework has already been employed in the field of vibration analysis to study rotationally symmetric systems like bladed disks (see Olson *et al.* [15] for a review in this context). This method allows us to compute multi-modal fluid instabilities, i.e., modal solutions that are spatially periodic over the array of n units, despite not being periodic over individual units, without solving the whole eigenvalue problem. Using this formalism, secondary stability analyses can be carried out on very large systems, allowing us to capture modes with small detuning factors spanning several wavelengths of the primary disturbance or resonances.

We present here an application of this framework to secondary stability theory of a swept boundary layer subject to stationary cross-flow modes. In this case the spatial periodicity, necessary for the application of the method, results from the periodicity of the primary disturbance, and not from the spatial recurrence of a geometric feature as for the examples provided in Schmid *et al.* [14]. The case of the swept boundary layer subject to stationary cross-flow modes has been chosen due to previous observation of long-wavelength structures in numerical and experimental studies. In fact, in a DNS study of such a flow case [16], detuning of the secondary instability appeared, but it was not further investigated. Moreover, long-wavelength coherent flow structures have been experimentally reported by [17], but their physical origin remained unclear. Finally, to the authors' knowledge, despite the extensive literature on the secondary instabilities in swept boundary layers [9,10,17–19], no study has considered yet the simultaneous secondary instability of a large number of cross-flow vortices. Moreover, for small spanwise wavelength instabilities, a direct comparison can be made with results from the Floquet analysis of Fischer and Dallmann [9], allowing a validation of the results. The outline of the remainder of the paper is as follows. The mathematical framework described in Schmid *et al.* [14] will be adapted for the study of secondary instabilities in Sec. II. The results and discussion on the secondary stability of the swept boundary layer are contained in Sec. III. The main findings are summarized in Sec. IV.

II. MATHEMATICAL FRAMEWORK

Let us consider a general, time-evolving system of the form

$$\frac{\partial \mathbf{Q}}{\partial t} = \mathbf{F}[\mathbf{Q}(\mathbf{x}, t)], \tag{1}$$

where $\mathbf{Q}$ is the state vector, $\mathbf{F}$ a nonlinear operator, and $\mathbf{x} = (x, y, z)$ is the spatial coordinates vector, with x being the streamwise, y the wall-normal, and z the spanwise direction. The flow is decomposed into a base flow $\mathbf{Q}_0(y)$, assumed to be locally parallel, and a small primary disturbance $\mathbf{q}_1(\mathbf{x}, t)$, such that $\mathbf{Q}(\mathbf{x}, t) = \mathbf{Q}_0(y) + \mathbf{q}_1(\mathbf{x}, t)$. Substituting the previous decomposition into Eq. (1) and neglecting nonlinear terms results in the following system for the perturbation:

$$\frac{\partial \mathbf{q}_1}{\partial t} = \mathbf{A}\mathbf{q}_1 \tag{2}$$

with $\mathbf{A}$ the Jacobian of the system. Assuming an ansatz of the form $\mathbf{q}_1(\mathbf{x},t) = \tilde{\mathbf{q}}_1(y)\exp[i(\alpha x + \beta z - \omega t)]$, modal and nonmodal stability analysis [1] can be performed, identifying specific waves of interest, with (α,β) the spatial and ω the temporal wave number. Notice that the primary instability analysis is carried out in a temporal framework, so that α,β are real quantities whereas $\omega = \omega_r + i\omega_i$ is complex.

Following Herbert [7], the secondary base flow $\mathbf{Q}_1$ is defined as the superposition of the primary disturbance of interest $\mathbf{q}_1$, with amplitude A, and the primary base flow $\mathbf{Q}_0$, such that $\mathbf{Q}_1(\mathbf{x},t) = \mathbf{Q}_0(y) + A\mathbf{q}_1(\mathbf{x},t)$. We also introduce a Galilean coordinate system (x_v, y, z_v) normal to the wave vector $\mathbf{k} = (\alpha,\beta)^T$ of the primary disturbance moving with phase speed $c = \omega_r/||\mathbf{k}||$ in the z_v direction. The passage from one coordinate system to the other can be performed through the following Squire transform: $x_v(t) = \beta/||\mathbf{k}||x - \alpha/||\mathbf{k}||z$ and $z_v(t) = \alpha/||\mathbf{k}||x + \beta/||\mathbf{k}||z - ct$. In this frame the secondary base flow $\mathbf{Q}_1(y,z_v)$ is stationary, streamwise independent, and $2\pi/||\mathbf{k}||$-periodic in the spanwise direction z_v. In the wave-oriented reference frame, the flow is decomposed into the secondary base flow $\mathbf{Q}_1(y,z_v)$ and a small secondary perturbation $\mathbf{q}_2(x_v,y,z_v,t)$ such as $\mathbf{Q}(x_v,y,z_v,t) = \mathbf{Q}_1(y,z_v) + \mathbf{q}_2(x_v,y,z_v,t)$. This formulation requires the shape assumption to be valid. Potentially, the base flow for secondary stability analysis can be retrieved by other means, such as parabolized stability equations or direct extraction from a numerical simulation. The key point is to guarantee the spatial periodicity of the secondary base flow on the subunits. Modal secondary perturbations are assumed:

$$\mathbf{q}_2(x_v,y,z_v,t) = \tilde{\mathbf{q}}_2(y,z_v)\exp(i\alpha_v x_v + \sigma t) \tag{3}$$

with α_v and $\sigma = \sigma_r + i\sigma_i$ being respectively the (real) streamwise wave number and the (complex) temporal wave number, σ_r the growth rate, and σ_i the circular frequency of the modes.

In the classical theory of secondary stability, Floquet analysis would be applied on the secondary base flow $\mathbf{Q}_1$. Instead, we consider a fluid system composed of the repetition in the spanwise direction z_v of the secondary base flow $\mathbf{Q}_1$ over n subunits of length $2\pi/||\mathbf{k}||$. The Navier-Stokes equations are then linearized around the $2\pi/||\mathbf{k}||$-periodic base flow $\mathbf{Q}_1(y,z_v)$. The ansatz for the secondary disturbance is introduced, yielding a two-dimensional local stability problem with $2\pi/||\mathbf{k}||$-periodic coefficients. The equations for the stability problem linearized around a two-dimensional stationary base flow $\mathbf{Q}_1(y,z_v) = [U_1(y,z_v), V_1(y,z_v), W_1(y,z_v)]^T$ can be found in Loiseau [20] and are reproduced here for the sake of clarity:

$$\begin{aligned}
\sigma\tilde{u}_2 + i\alpha_v U_1\tilde{u}_2 + V_1\partial_y\tilde{u}_2 + W_1\partial_{z_v}\tilde{u}_2 + \tilde{v}_2\partial_y U_1 + \tilde{w}_2\partial_{z_v}U_1 &= -i\alpha_v\tilde{p} + \frac{1}{\mathrm{Re}}\left(\partial_{yy} + \partial_{z_v z_v} - \alpha_v^2\right)\tilde{u}_2\\
\sigma\tilde{v}_2 + i\alpha_v U_1\tilde{v}_2 + V_1\partial_y\tilde{v}_2 + W_1\partial_{z_v}\tilde{v}_2 + \tilde{v}_2\partial_y V_1 + \tilde{w}_2\partial_{z_v}V_1 &= -\partial_y\tilde{p} + \frac{1}{\mathrm{Re}}\left(\partial_{yy} + \partial_{z_v z_v} - \alpha_v^2\right)\tilde{v}_2\\
\sigma\tilde{w}_2 + i\alpha_v U_1\tilde{w}_2 + V_1\partial_y\tilde{w}_2 + W_1\partial_{z_v}\tilde{w}_2 + \tilde{v}_2\partial_y W_1 + \tilde{w}_2\partial_{z_v}W_1 &= -\partial_{z_v}\tilde{p} + \frac{1}{\mathrm{Re}}\left(\partial_{yy} + \partial_{z_v z_v} - \alpha_v^2\right)\tilde{w}_2\\
i\alpha_v\tilde{u}_2 + \partial_y\tilde{v}_2 + \partial_{z_v}\tilde{w}_2 &= 0,
\end{aligned} \tag{4}$$

where Re is the Reynolds number. Performing a classical linear stability analysis of a system of this size yields a prohibitive computational cost. However, this task can be tackled at an affordable cost using the framework described by Schmid *et al.* [14]. For the sake of completeness, the method will be quickly described in the following. The first step consists in reordering the system, which is partitioned into n smaller systems, each one corresponding to a subunit. Mathematically, the

disturbance equations can be recast under the following form:

$$\frac{\partial}{\partial t}\begin{pmatrix} \mathbf{q}_2^{(0)} \\ \mathbf{q}_2^{(1)} \\ \vdots \\ \mathbf{q}_2^{(n-1)} \end{pmatrix} = \underbrace{\begin{pmatrix} \mathbf{A}^{(0)} & \mathbf{A}^{(1)} & \cdots & \mathbf{A}^{(n-1)} \\ \mathbf{A}^{(n-1)} & \mathbf{A}^{(0)} & \cdots & \mathbf{A}^{(n-2)} \\ \vdots & \vdots & & \vdots \\ \mathbf{A}^{(1)} & \mathbf{A}^{(2)} & \cdots & \mathbf{A}^{(0)} \end{pmatrix}}_{\mathbf{A}'} \underbrace{\begin{pmatrix} \mathbf{q}_2^{(0)} \\ \mathbf{q}_2^{(1)} \\ \vdots \\ \mathbf{q}_2^{(n-1)} \end{pmatrix}}_{\mathbf{q}_2} \tag{5}$$

with $\mathbf{A}'$ the Jacobian associated with the full secondary stability problem, which is composed of the matrices $\mathbf{A}^{(0)}$ and $\mathbf{A}^{(j)}$ (for $j = 0, \ldots, n-1$) describing respectively the dynamics in a subunit and the coupling interactions between subunits. The secondary disturbance state vector in the jth subunit is denoted as $\mathbf{q}_2^{(j)}$. The Jacobian matrix $\mathbf{A}'$ is block-circulant due to the specific n-periodic nature of the system and can become a block-diagonal matrix $\hat{\mathbf{A}}$ through the similarity transformation:

$$\mathbf{P}^H \mathbf{A}' \mathbf{P} = \mathrm{diag}(\hat{\mathbf{A}}^{(0)}, \hat{\mathbf{A}}^{(1)}, \ldots, \hat{\mathbf{A}}^{(n-1)}) \equiv \hat{\mathbf{A}}. \tag{6}$$

The transfer matrix $\mathbf{P}$ can be found analytically as

$$\mathbf{P} = \mathbf{J} \otimes \mathbf{I} \tag{7}$$

with $\mathbf{J}$ a matrix such as $\mathbf{J}_{j+1,k+1} = \rho_j^k/\sqrt{n}$ for $j, k = 0, \ldots, n-1$ and $\rho_j = \exp(2i\pi j/n)$ the jth of the n roots of unity. The symbol $\otimes$ denotes the usual Kronecker product and $\mathbf{I}$ the identity matrix. With this transformation, the linear stability problem has been reduced to the study of n smaller subsystems characterized by the matrices $\hat{\mathbf{A}}^{(j)}$. Hence, the full spectrum of the matrix $\mathbf{A}'$ can be found merging the n spectra of $\hat{\mathbf{A}}^{(j)}$ for $j = 0, \ldots, n-1$. Similarly, provided $\mathbf{v}_j$ is an eigenvector of $\hat{\mathbf{A}}^{(j)}$, the eigenfunctions of the full system can be retrieved and take the form $[\mathbf{v}_j, \rho_j \mathbf{v}_j, \rho_j^2 \mathbf{v}_j, \ldots, \rho_j^{n-1} \mathbf{v}_j]^T$ for $j = 0, \ldots, n-1$. In the case of nearest-neighbor coupling, rather common in many applications, the Jacobian $\mathbf{A}'$ reduces to a block-tridiagonal matrix. Only a three-unit system $\mathbf{A}^{(0)}, \mathbf{A}^{(1)}, \mathbf{A}^{(2)}$ needs to be discretized and processed, significantly reducing the complexity and computational cost of the method. A sensitivity study of the method with respect to the nearest-neighbor coupling hypothesis, as well to the number of subunits considered, is carried out in the Appendix.

Notice that the argument θ_j of the root-of-unity ρ_j acts as a phase shift between the different subunits: the farther it is from 0 (or 2π), the more desynchronized the secondary mode is. Thus, the eigenfunction $\mathbf{v}_j$, after each subunit, is phase shifted by $\theta_j = \arg(\rho_j) = 2\pi j/n$, meaning that after $n_j = 2\pi/\theta_j = n/j$, (here $j = 1, \ldots, n-1$) subunits, the cumulative phase shift will exceed 2π, giving an estimate of the effective fundamental period of the eigenfunction of the full system. Associated with this number of coupled subunits, the fundamental wave number of the mode can be retrieved and is equal to $\beta_v = 2\pi/(2\pi n_j/||\mathbf{k}||) = j||\mathbf{k}||/n$.

The connection with Floquet analysis and the corresponding detuning factor ϵ can be thus specified. In the wave-oriented frame, the secondary base flow is periodic with wave number $\beta_v^0 = ||\mathbf{k}||$ in the z_v direction. After Fourier expanding the base flow in this direction (see [1], for instance) the secondary disturbance has the following modal expansion:

$$\mathbf{q}_2(x_v, y, z_v, t) = e^{\sigma t} e^{i\alpha_v x_v} \sum_m \hat{\mathbf{q}}_m(y) e^{i(m+\epsilon)||k||z_v}, \tag{8}$$

where $\epsilon = \gamma_i/||\mathbf{k}||$, γ_i being the imaginary part of the classical Floquet exponent γ. The fundamental wave number ($m = 0$) of the resulting mode is thus $\beta_v = \epsilon||\mathbf{k}||$, which, after equating with the expression of β_v previously obtained for the jth eigenmode with root-of-unity ρ_j, gives $\epsilon = 1/n_j = j/n$. Reintroducing the detuning factor into the Floquet modal expansion

yields

$$\mathbf{q}_2^{(j)}(x_v, y, z_v, t) = e^{\sigma t} e^{i\alpha_v x_v} e^{ij\frac{||k||}{n} z_v} \sum_m \hat{\mathbf{q}}_m(y) e^{im||k||z_v} \tag{9}$$

$$= e^{\sigma t} e^{i\alpha_v x_v} e^{ij\frac{||k||}{n} z_v} \tilde{\mathbf{q}}(y, z_v) \tag{10}$$

for $j = 0, \ldots, n-1$, where the Bloch theorem for the n subunits is retrieved.

Comparing the computational cost of the Bloch wave method to that of a limited [$O(10)$] number of Floquet computations with different detuning factors, one can conclude that the total CPU time is approximately equivalent. Thus, there is not a direct computational advantage of using such a method instead of Floquet analysis.

However, in the present framework, the eigenproblem is solved using a two-dimensional base flow, without needing to develop and truncate it in a Fourier series. This can be quite beneficial in the case of complex base flows (as mean flows), where using Fourier modes may not be convenient if the secondary base flow has been computed using a nonspectral method (e.g., a finite-difference numerical code). Of course, this would merely constitute a pragmatic advantage, while the two approaches are equivalent from both a theoretical and computational point of view. Finally, since a large numbers of eigenmodes can be retrieved, the framework is also well suited for carrying out nonmodal or resolvent analyses. These have not been described as the present article focuses on modal instabilites. For a full discussion, the reader is referred to Schmid *et al.* [14].

III. RESULTS

To illustrate the previous method, the secondary instability of stationary cross-flow vortices in a swept-boundary flow is investigated. This analysis extends and completes the work of Fischer and Dallmann [9], where long-wavelength instabilities were not investigated. All the stability results hereafter are obtained using a temporal approach ($\omega, \sigma \in \mathbb{C}$). The secondary stability problem is tackled considering the nearest-neighbor coupling assumption (see the Appendix for a validation of this assumption). For both primary and secondary analyses, the stability problem is discretized with a spectral collocation method [22]. Wall-normal and spanwise directions are respectively discretized with a 64-point Chebyschev grid and a 64-point Fourier grid, respectively. The generalized eigenvalue problem is solved using a Krylov-Schur algorithm of the SciPy Python module coupled with a shift-and-inverse technique.

A. Primary stability analysis

In the following, we consider the incompressible flow over an infinite swept flat plate with an imposed negative pressure gradient (i.e., decreasing pressure in the chordwise direction). The laminar base flow $\mathbf{Q}_0 = [U_0(y), 0, W_0(y)]^T$ is modeled with a Falkner-Skan-Cook profile [23,24]. Precisely, introducing f and g such that $U_0(y) = f'(y)\cos\theta$ and $W_0(y) = g(y)\sin\theta$, we have

$$(2 - \beta_H) f''' + f f'' + \beta_H [1 - (f')^2] = 0, \tag{11}$$

$$(2 - \beta_H) g'' + f g' = 0, \tag{12}$$

where the Hartree dimensionless pressure-gradient parameter (β_H), the local sweep angle, and the local Reynolds number are set respectively to $\beta_H = 0.630$, $\theta = 46.9^\circ$, and $\mathrm{Re} = \mathrm{Re}_\delta = 826$. These parameters are taken directly from Fischer and Dallmann [9] and set to fit qualitatively experimental results from Müller [25]. Assuming wavelike solutions for the disturbances, modal stability analysis is performed for this configuration. Stationary disturbances maximizing the temporal growth rate with respect to the streamwise and spanwise wave numbers α and β are sought. Figure 1 exhibits the neutral curve of the primary instability. Since Squire's theorem is not valid for three-dimensional flows [26], the $\beta < 0$ plane was also investigated for the sake of completeness. The maximum growth rate for stationary disturbances is reached for $(\alpha, \beta) = (0.0361, 0.4774)$. The eigenfunctions

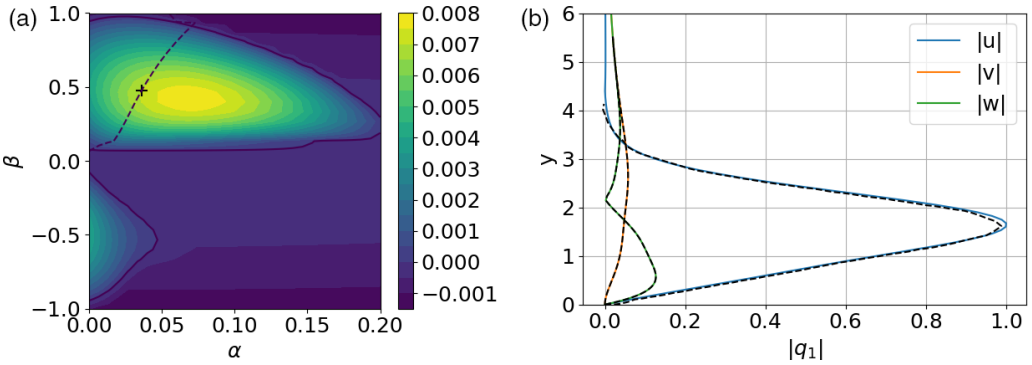

FIG. 1. (a) Neutral curve [black solid line $\omega_i(\alpha, \beta) = 0$] of the swept boundary layer for $\mathrm{Re}_\delta = 826$. The dashed line corresponds to stationary disturbances, $\omega_r(\alpha, \beta) = 0$. (b) Absolute value of the eigenfunctions for $\mathrm{Re}_\delta = 826$, $\alpha = 0.0361$, and $\beta = 0.4774$ [$\Psi = \arctan(\beta/\alpha) = 89.9°$]. The dashed lines are extracted from Fischer and Dallmann [9].

of this mode are displayed in Fig. 1(a). A second instability region appears as well, albeit with lower growth rates and no stationary disturbances. The agreement with the results found in Fischer and Dallmann [9] is excellent.

B. Secondary stability analysis

Secondary stability of the flow is investigated using the framework described in Sec. II. The secondary base flow is defined as $\mathbf{Q}_1(y, z_v) = \mathbf{Q}_0(y) + A\mathbf{q}_1(y, z_v)$ with $\mathbf{q}_1$ the disturbance with wave vector $\mathbf{k} = (\alpha, \beta) = (0.0361, 0.4774)^T$ in the original reference frame. The amplitude A is set as $A = 0.0789$ [9]. The resulting base flow on one subunit and in the wave-oriented reference frame is shown in Fig. 2. Qualitative validity of the shape assumption in this particular case is shown through comparison with experiments in Fischer and Dallmann [9]. Regarding the saturation amplitude, in a similar configuration, White and Saric [27] found a saturation amplitude of 19% for subcritical transition. This has been retrieved in the more recent work of Serpieri and Kotsonis [17] where, at worst, an N factor of 3 was found, corresponding to a saturation amplitude of 20%. Returning to the study of White and Saric [27], in the case where the generated primary cross-flow vortices were

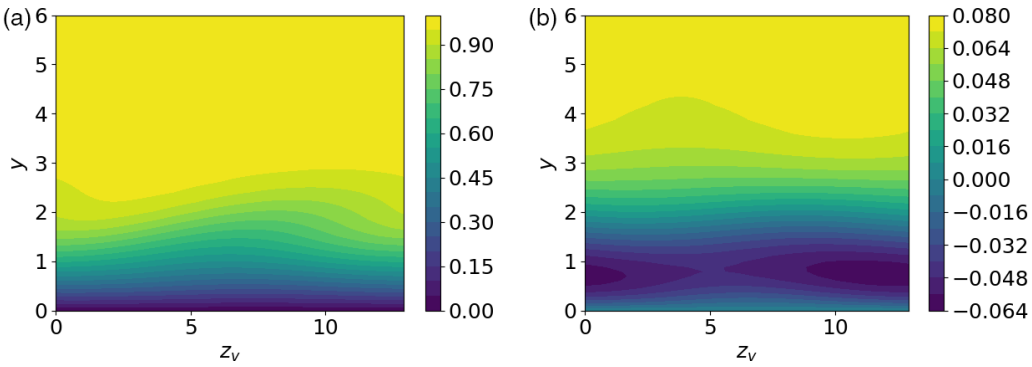

FIG. 2. Secondary base flow $U_1(y, z_v)$ (a) and $W_1(y, z_v)$ (b) in the wave-oriented reference frame for one subunit. The wall-normal component V_1 is nonzero but is one order of magnitude smaller than W_1, thus it is not shown.

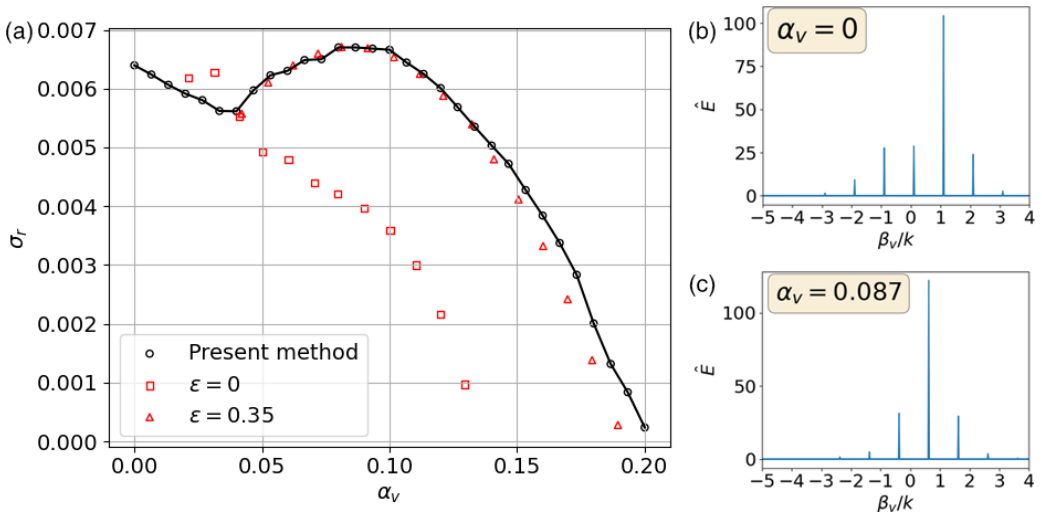

FIG. 3. (a) Evolution of the secondary growth rate σ_r (black circles) as a function of the streamwise wave number α_v. A comparison is made with Fig. 8 of Fischer and Dallmann [9] (red symbols), where ϵ corresponds to the detuning factor of the Floquet analysis [9]. (b), (c) Spatial Fourier spectra of the energy of the most unstable mode for $\alpha_v = 0$ (b) and $\alpha_v = 0.087$ (c).

supercritical, their amplitude grew by only a few percent before reaching saturation, in agreement with the chosen amplitude.

Secondary growth rate for the full system as a function of the streamwise wave number is displayed in Fig. 3. Two modes appear to compete: the maximum growth rate $\sigma_r = 0.0068$ is reached for $\alpha_v = 0.087$, while streamwise independent perturbations ($\alpha_v = 0$) also display strong amplification with $\sigma_r = 0.0065$. A direct comparison can be made with Fig. 8 from Fischer and Dallmann [9], where Floquet analysis (on one subunit) is conducted for both harmonic modes and resonant modes with a detuning factor $\epsilon = 0.35$, where $\epsilon = \gamma_i/||\mathbf{k}||$ and γ_i is the imaginary part of the Floquet exponent γ, as discussed in Sec. II. Maximum growth rates are obtained for $\alpha_v = 0.03$ and $\alpha_v = 0.087$, respectively. The agreement with the $\epsilon = 0.35$ curve is good although some discrepancies are observed for the growth rates of harmonic modes. The Floquet analysis seems to overestimate the secondary growth rate in the range where small wave number modes are predominant.

The nature of the instabilities obtained in our framework can be inferred inspecting the spatial Fourier energy spectra of the most unstable modes. These Fourier spectra, realized for the cases with $\alpha_v = 0$ and $\alpha_v = 0.087$, are shown in Figs. 3(b) and 3(c). The detuning factor can be identified, from the spectra, as $\epsilon = \beta_v/\|\mathbf{k}\|$ with β_v the wave number of the Fourier fundamental mode. Thus, the maximum at $\alpha_v = 0.087$ is associated with a detuned mode with $\epsilon = 0.35$, in agreement with Fischer and Dallmann [9]. For $\alpha_v = 0$, all the frequencies are almost multiples of $\|\mathbf{k}\|$, indicating a quasifundamental ($\epsilon = 0.08$) nature of the instability. It is also worth noticing the larger number of modes required to accurately describe the instability. The secondary perturbation is truly multimodal with important coupling effects between subunits. Notice that Fischer and Dallmann [9] missed this secondary mode, since the associated value of ϵ is very low, but still not zero.

The spectra for the system composed of $n = 50$ subunits and for $\alpha_v = 0$ and $\alpha_v = 0.087$ are displayed in Fig. 4. A high number of subunits corresponds to a (very) large system and allows a wide range of admissible spanwise wave numbers. This explains the appearance of many branches within the spectra. The higher the number of subunits, the more continuous these branches will be. Quasihorizontal branches represent convective Squire modes and do not play a role in the asymptotic stability as they are always stable. The eigenvalues are colored with the argument of

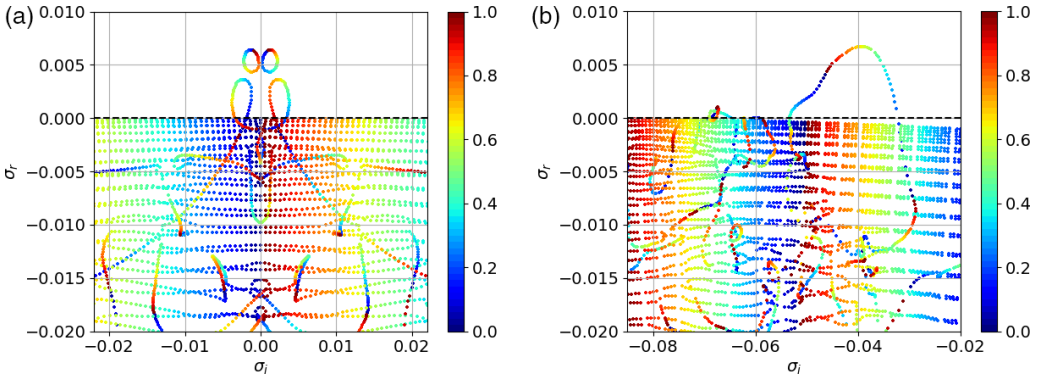

FIG. 4. Full spectra of the secondary stability problem for $\mathrm{Re}_\delta = 826$, $A = 0.0789$, $n = 50$ and for $\alpha_v = 0$ (a) and $\alpha_v = 0.087$ (b). The full spectrum is constructed merging the n spectra of the subsystems. The eigenvalues have been colored by the argument of their respective root of unity: $z \in [0, 1]$ such as $\rho = \exp(2i\pi z)$. The dashed line corresponds to the $\sigma_r = 0$ line.

their corresponding root-of-unity ρ_j. Brighter colors indicate important phase shift between subunits and, thus, strong desynchronization of the perturbation. For $\alpha_v = 0$, as expected, the spectrum is symmetric with respect to the $\sigma_i = 0$ axis. Two unstable branches are found: the most unstable one loops on itself, and the second remains open ended. The maximum growth rate is reached for $\rho_4 = 0.87 + 0.48\,j$, corresponding to a phase shift $\theta = 29^o$ between the subunits and indicating limited desynchronization. The spectrum for $\alpha_v = 0.087$ is quite different. Two unstable branches are also observed. The first is marginally stable, and reaches a maximum growth rate for synchronized modes. The second is much more unstable and reaches a maximum for $\rho_{31} = -0.73 - 0.68\,j$, equivalent to a phase shift $\theta = -137^o$ and causing strong desynchronization.

The most unstable modes are reconstructed for $\alpha_v = 0$ and $\alpha_v = 0.087$. Figure 5 displays the streamwise component of the disturbance velocity in the full domain, while Fig. 6 exhibits the cross-flow velocities for a group of three subunits. The streamwise velocity disturbance is one order of magnitude higher than the cross-flow components. The position of the maxima of the streamwise disturbance slightly varies across the subunits, although it is approximately located on the upwelling of the wave pattern of the secondary base flow. The detuned behavior can be observed in both modes: for $\alpha_v = 0$, approximately 23 subunits are involved in large-wavelength oscillations, whereas only three contribute to the instability for $\alpha_v = 0.087$. The beating phenomenon observed for $\alpha_v = 0$ is characteristic of a superposition of functions with two close spatial wavelengths, one of these being the spatial wavelength of the primary cross-flow vortices, which, in this context, acts as a forcing.

The cross-flow dynamics, displayed in Fig. 6 on a group of three subunits, is less sensitive to unit-to-unit variation, likely due to the smaller magnitude of the components. The streamwise-independent mode displays counter-rotating vortices, which might be linked to either the lift-up effect or to a Görtler instability [28]. The latter is usually linked to curved walls, but it has been conjectured that the curvature of the base flow streamlines could have a similar effect on the instability of a boundary layer. Since the lift-up is usually a nonmodal energy growth mechanism, while here we focus on modal instabilities, a Görtler-like instability can be a good candidate for explaining the onset of such counter-rotating vortices on top of the curved streamlines induced by the primary modes.

For $\alpha_v = 0.087$, the vortical structures are sensibly different. The vortices seem to arise from the roll-up of a shear layer. This might have been anticipated, since it has been shown that secondary instability of swept flows can be related to Kelvin-Helmholtz instabilities [19]. Furthermore, these secondary vortices are located on the edge of the boundary layer, in a region associated with strong wall-normal and spanwise shear layers. Ultimately, it appears that two distinct mechanisms are at play. The first is linked to streak instabilities, which push high-velocity fluid downwards near the

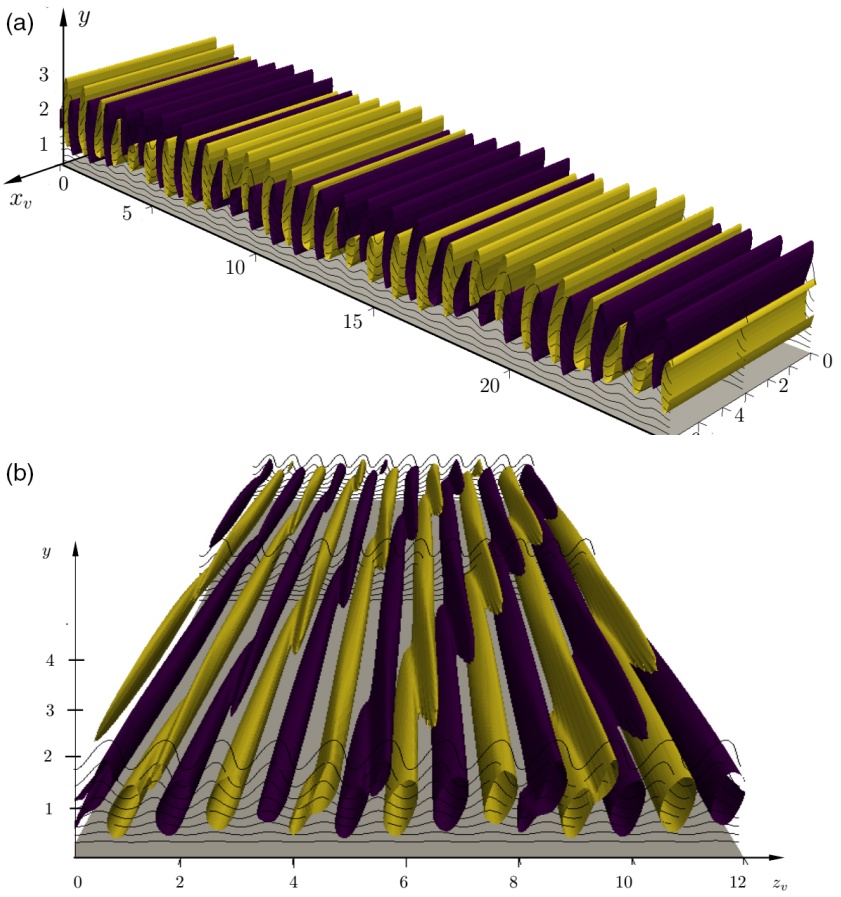

FIG. 5. Three-dimensional views of the streamwise velocity component of the most unstable mode for different streamwise wave number α_v (a: $\alpha_v = 0$, $n = 25$; b: $\alpha_v = 0.087$, $n = 12$) and a number of visualized subunits n, chosen in both cases to give a good overview of the spatial characteristics of the mode. Isosurfaces correspond to $\pm 0.75 u_{\max}$. Spanwise direction is normalized by the spatial period of a subunit $2\pi/||\mathbf{k}||$. Notice the beating phenomenon for $\alpha_v = 0$.

walls while low-velocity fluid from the near-wall region is ejected higher in the boundary layer. The second instability mechanism is Kelvin-Helmholtz related and generates secondary vortices through the roll-up of the shear layer located at the edge of the boundary layer.

In an effort to assess more precisely the instability nature of these two modes, a comparison can be made with experimental work [17,29] in which a POD decomposition of the laminar-turbulent transition on a swept wing was realized. The most energetic POD mode appeared to be streamwise-independent, with a shape similar to that found in the present analysis. Furthermore, it was characterized by a very low frequency in the [1 Hz, 20 Hz] range, in agreement with the frequency $f = 4$ Hz found here for the $\alpha_v = 0$ mode. However, no modulation of the mode has been observed as the POD was realized for only one cross-flow vortex. Figure 7 depicts the absolute value of the streamwise component of the disturbance. For $\alpha_v = 0.087$, the concentration of the streamwise velocity disturbance in the bottom part of the cross-flow vortices is reminiscent of a type III instability [29]. The frequency $f = 154$ Hz obtained for this mode is smaller than the frequency range 350 Hz $\leqslant f \leqslant$ 550 Hz found by Serpieri [29] but still in good agreement with the frequency $f = 145$ Hz found by Fischer and Dallmann [9]. This type of mode is traditionally associated with

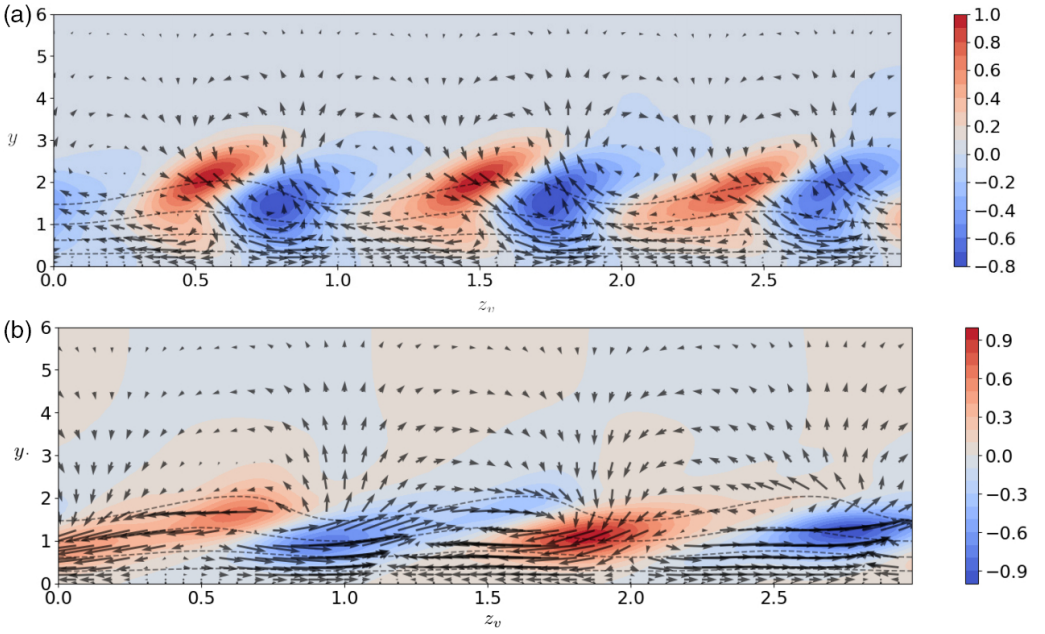

FIG. 6. Vectors: cross-flow velocity in the plane (y, z_v) for a group of three subunits. The contour plot represents the streamwise component of the secondary base flow. The flow in the z direction goes from left to right. (a) $\alpha_v = 0$; (b) $\alpha_v = 0.087$.

interactions between primary stationary and traveling modes. The $\alpha_v = 0$ mode is quite interesting: the streamwise component of the perturbation is located on the upwelling of the cross-flow vortex which is characteristic of a type I instability. The mode is also strongly correlated with the spanwise gradient of the base flow, as for type I modes. However, these are usually associated with nonzero streamwise wave number and higher frequencies.

In order to assess more precisely the nature of the $\alpha_v = 0$ mode, the amplitude A of the primary disturbance was varied. Figure 8 displays the evolution of the spectrum of the $\alpha_v = 0$ mode for different amplitudes. When $A \to 0$, characteristics of the primary instability are retrieved: the

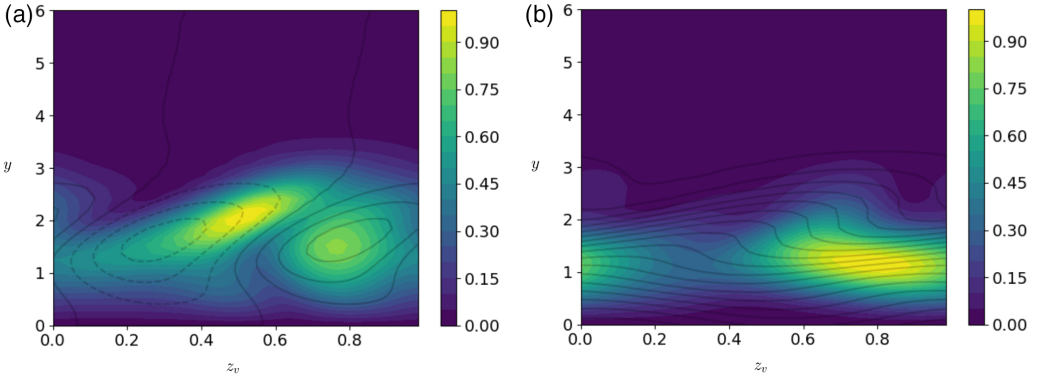

FIG. 7. Absolute value of the streamwise component of the eigenfunction for $\alpha_v = 0$ (a) and $\alpha_v = 0.087$ (b). The solid contours depict the spanwise and wall-normal velocity gradients of the secondary base flow, respectively.

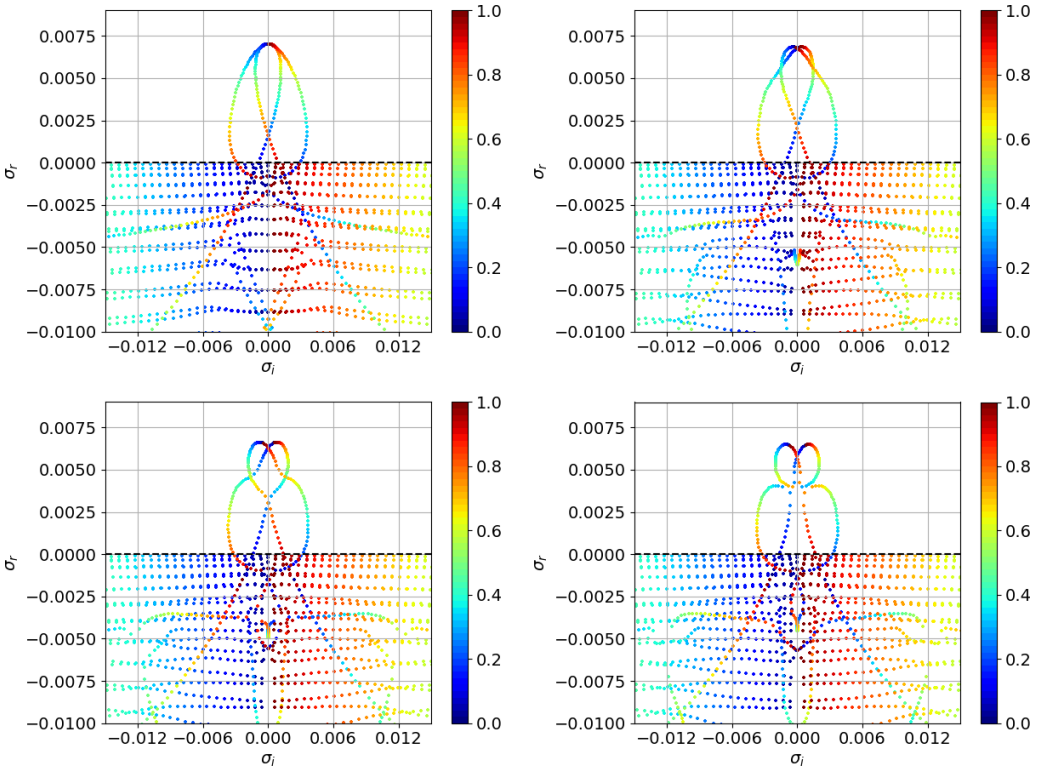

FIG. 8. Spectra of the secondary stability problem for $\mathrm{Re}_\delta = 826$, $n = 50$, $\alpha_v = 0$ and for several amplitudes A. From left to right and top to bottom: $A = 0.02$, $A = 0.04$, $A = 0.06$, and $A = 0.07$. The dashed line corresponds to the $\sigma_r = 0$ line.

primary growth rate is reached for stationary cross-flow vortices. However, this mode results from the merging of two spatial branches, forming an exceptional point [30]. Exceptional points are spectral singularities in the parameter space of a system in which two or more eigenvalues, and their corresponding eigenvectors, simultaneously coalesce and are usually associated with strong interactions between modes like resonances [21]. In the present case, the exceptional point indicates the presence of interactions between cross-flow vortices with different spanwise wave numbers as can be seen for $A = 0.06$, from the two eigenfunctions shown in Fig. 9. When the amplitude is increased, the outer branch is deformed, leading to the formation of two other exceptional points associated with interactions between traveling disturbances with opposite spanwise wave numbers. For $A = 0.07$, a change in the topology of the spectrum can be observed: the two spatial branches break up, then reconnect in a different configuration, forming the loops observed in the spectrum of Fig. 4. This evolution of the spectrum tends to indicate a change in the nature of the modes. However, it may be noticed that the growth rate of this mode remains finite as the amplitude of the base flow primary instability continuously reduces to some small but finite threshold. Thus, the topological changes within the spectrum should be linked to the modulation effect provided by the increase in amplitude of the primary instability. The resulting eigenvectors are visualized together with the modulated base flow for $A = 0.02$ and $A = 0.07$. On the contrary, carrying out the same analysis for the $\alpha_v = 0.087$ mode as shown in Fig. 10, only a continuous deformation of the unstable branch can be observed. Streamwise velocity eigenfunctions of the most unstable mode are provided in Fig. 11 for different amplitudes. The most unstable mode is found for $\epsilon \approx 0.35$ in all cases, yielding a secondary instability coupling approximately three subunits. Besides, it appears

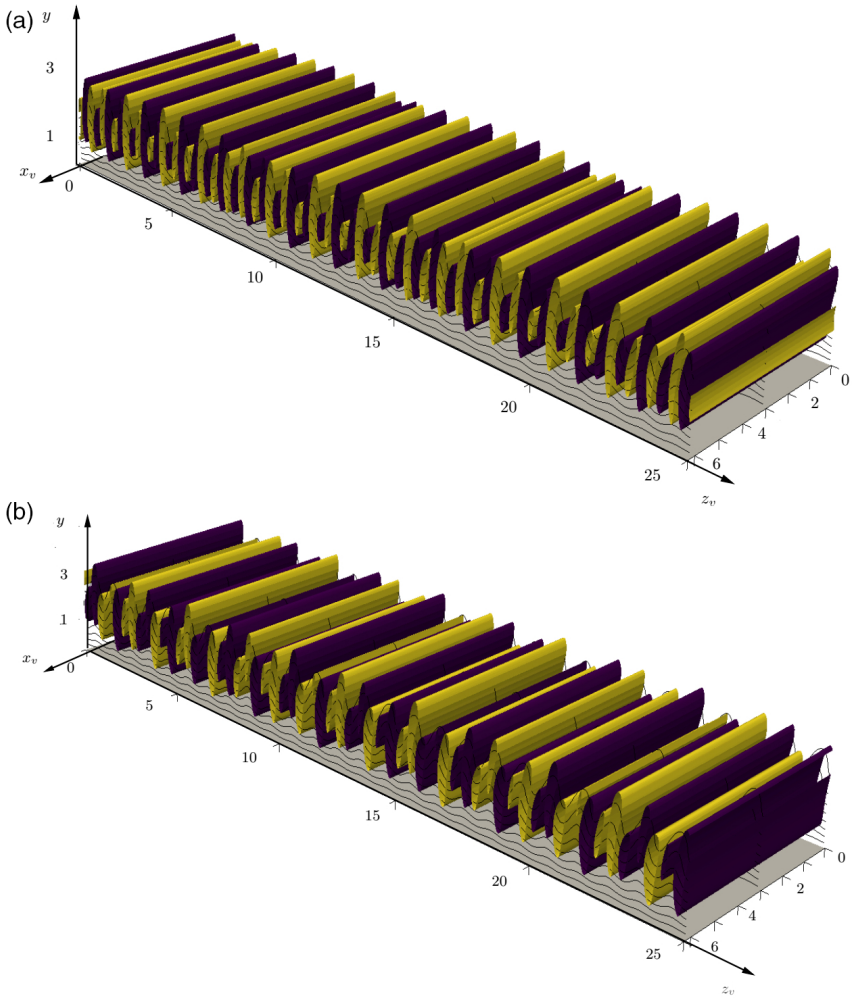

FIG. 9. Three-dimensional views of the streamwise velocity perturbation of the unstable modes at the exceptional point for $\alpha_v = 0$, $A = 0.06$, and $n = 25$ subunits. Isosurfaces correspond to $\pm 0.75 u_{\max}$. Spanwise direction is normalized by the spatial period of a subunit $2\pi/||\mathbf{k}||$. Notice the beating phenomenon for $\alpha_v = 0$. (a) ρ_{22}; (b) ρ_{35}.

to stem from a traveling cross-flow mode, which is progressively deformed by the presence of the primary stationary cross-flow mode. The traveling cross-flow mode has a spatial periodicity approximately three times larger than the primary mode. This is in agreement with the findings of Malik *et al.* [31], who argued, using an NPSE approach, that the modulation is simply a result of the nonlinear interaction of the stationary and traveling disturbances that becomes more pronounced as the amplitude A is increased.

IV. CONCLUSIONS

A formulation for secondary stability analysis of linearly unstable flows has been proposed, which allows retrieving amplification mechanisms involving detuned modes spanning several units of the primary instability. Such a method is based on the combination of a local two-dimensional stability analysis and a Bloch waves formalism originally described in Schmid *et al.* [14]. Within

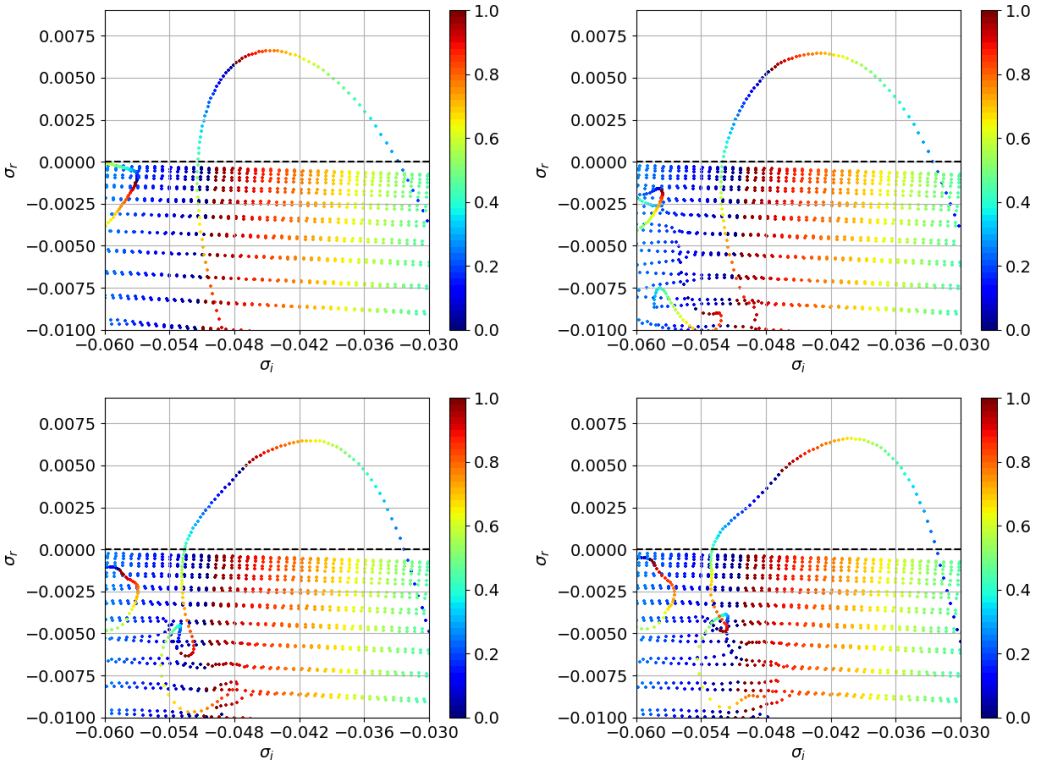

FIG. 10. Same as Fig. 8 but for the $\alpha_v = 0.087$ mode.

this framework, the linear stability of systems having a high number of degrees of freedom resulting from the repetition of several units of the primary instability is investigated.

Using this method, the secondary stability of a swept boundary layer developing steady cross-flow vortices has been investigated. This flow case has been chosen due to previous observation of

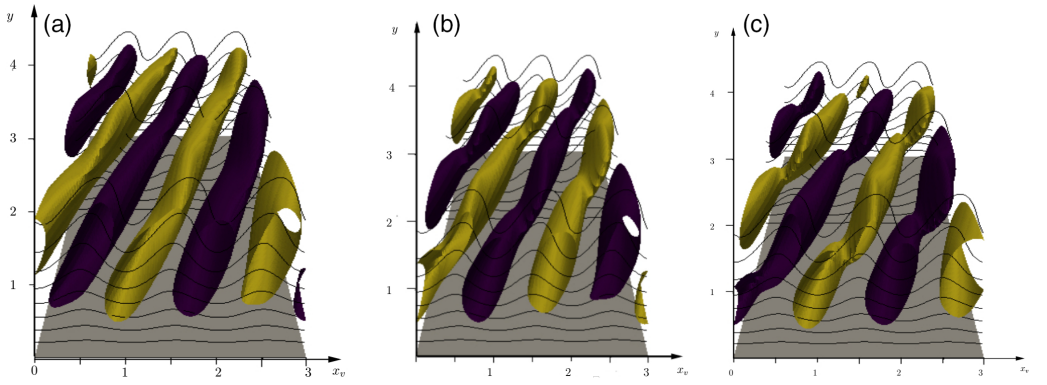

FIG. 11. Three-dimensional views of the streamwise velocity perturbation of the most unstable mode for $\alpha_v = 0.087$ and different amplitudes (a: $A = 0.02$; b: $A = 0.06$; c: $A = 0.07$). The number $n = 3$ of subunits visualized has been chosen to accommodate approximately one spatial period of the secondary mode ($\epsilon \approx 0.35$). Isosurfaces correspond to $\pm 0.75 u_{\max}$. Black contours represent the secondary base flow. Spanwise direction is normalized by the spatial period of a subunit $2\pi/||\mathbf{k}||$.

long-wavelength structures in numerical and experimental studies [16,17], whose physical origin remained unclear. Moreover, for this flow case a direct comparison with the Floquet analysis carried out by the work of Fischer and Dallmann [9] (limited to small to intermediate wavelengths) can be made for validation. Here we consider subunits composed of one cross-flow stationary vortex, thus neglecting small mistunings between neighboring vortices which might be responsible of mode localization [32–34], potentially leading to high-amplitude phenomena such as the jagged aspect of the transition front. Within the same framework, this limitation can be partially overcome by considering subunits composed of more than one cross-flow vortice, opportunely modulated in amplitude.

The instability dynamics seems to result from the competition between streamwise independent modes and detuned modes with detuning factor $\epsilon = 0.35$. In the case of streamwise wave numbers $\alpha_v > 0.087$, the secondary instability analysis can be accurately described by a low number of modes, and it has been previously retrieved by Floquet analysis, whereas, for smaller wave numbers, a multimodal instability arises, corresponding to a Floquet mode with very small detuning factor, that has been never reported in the literature to the best of our knowledge. The full spectra are retrieved, and unstable branches can be identified. Notably, for streamwise independent perturbations, large-wavelength oscillations can be seen, while a staggered pattern, characteristic of a subharmonic transition, appears in the disturbance for $\alpha_v = 0.087$. The wavelength of the staggered pattern is imposed by the detuning factor. Physically, two instability mechanisms have been identified: one linked to streaks and the circulation of high-momentum fluid towards the edge of the boundary layer. The other one appears linked to the roll-up of a shear layer and seems related to Kelvin-Helmholtz instabilities.

Notably, the obtained secondary disturbances show some similarities with the POD modes experimentally retrieved previously [17,29]. A direct comparison with these experimental findings has allowed us to assess the nature of these secondary perturbations. In particular, the $\alpha_v = 0$ mode resembles a type I mode, while the $\alpha_v = 0.087$ disturbance is clearly identified as a type III mode, which has been related to interactions between stationary and traveling cross-flow vortices. Often this disturbance is considered as a modulation of the primary instability rather than a proper instability [31]. This possibility has been investigated by varying the amplitude of the primary disturbance: for the type III mode, the unstable branch continuously deforms as the amplitude is increased.

This approach has thus allowed the identification of two long-wavelength detuned instabilities that were observed in numerical and experimental literature studies. Light has been shed on the dynamics of detuned secondary modes with a small detuning factor, which have been overlooked in previous studies. However, they seem to play a role when the spatial wavelength of the secondary mode gets close to that of the base flow, yielding a long-wavelength beating phenomenon. It may be interesting to investigate the existence of detuned secondary instabilities of other canonical flows. In the case of cross-flow vortices, more accurate results could be obtained by using a nonlinearly saturated base flow. In general, studies on the secondary instability of fundamental coherent structures such as streaks could be completed and extended through the use of this framework.

ACKNOWLEDGMENTS

This work was granted access to the HPC resources of IDRIS under the allocation made by GENCI. This work has been partially funded by Grant No. P2022CZ5KZPNRR, “SLIPS: Slippery surfaces for drag reduction” of the Italian Ministry of University and Research (MUR). Finanziato dall’Unione europea – Next Generation EU.

APPENDIX

In this Appendix we carry out a sensitivity analysis of the results with respect to the main hypotheses of the method, namely, the use of the finite number of subunits, and the neighboring-coupling approach.

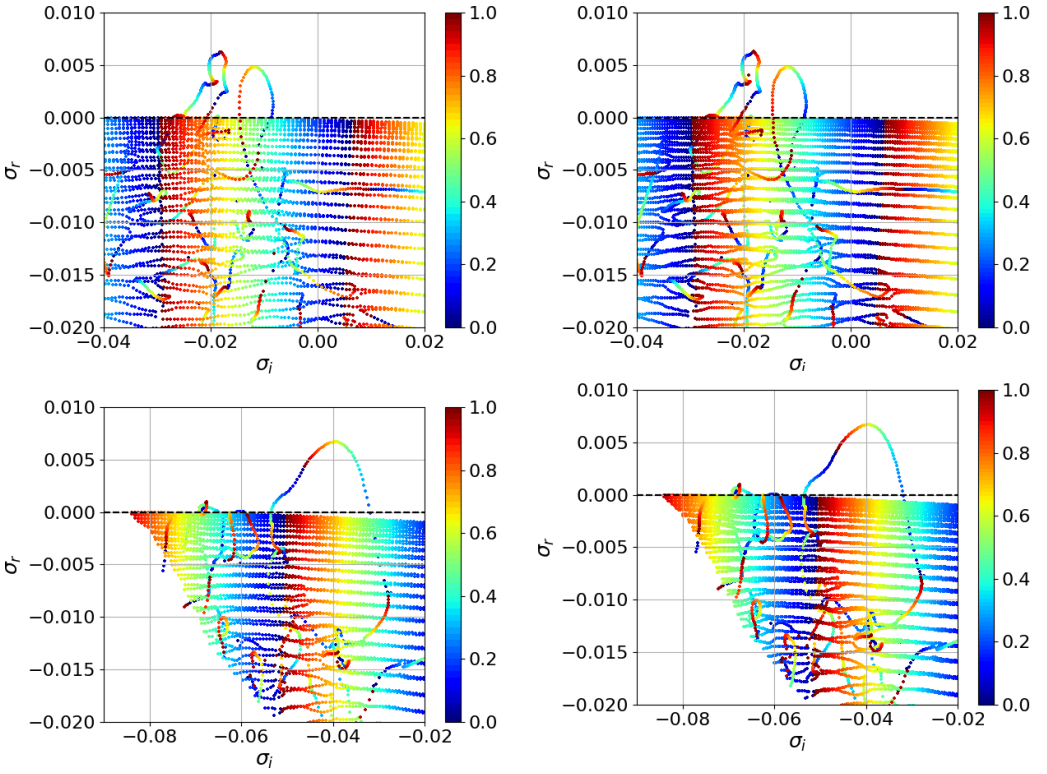

FIG. 12. Eigenvalue spectra for $\mathrm{Re}_\delta = 826$, $A = 0.0789$, $\alpha_v = 0.03$ (top row), and $\alpha_v = 0.0087$ (bottom row) with a number of subunits (left) $n = 50$ and (right) $n = 80$. The dashed line corresponds to the $\sigma_r = 0$ line.

First, in order to verify that the limited number of subunits does not affect strongly the results, we have carried out our computations with increasing number of subunits. In Fig. 12 we show the eigenvalue spectra for the cases $\alpha_v = 0.03$ (top row) and $\alpha_v = 0.0087$ (bottom row) with $n = 50$ (left) and $n = 80$ (right) subunits. The spectra are practically identical. Thus, provided that the number of subunits is sufficiently high (here $n > 50$), the finite number of subunits has virtually no effect on the results.

Concerning the nearest-neighbor coupling approach, we have increased for a few cases the number of coupled units, from $N_u = 3$ to $N_u = 50$. For the case $\alpha_v = 0.030$, which has $\rho = 0$ (fundamental instability), the growth rate does not change at all, as expected. For the detuned cases with $\alpha_v = 0.030$, $\rho = 48$ and $\alpha_v = 0.087$, $\rho = 30$, the maximum growth rate varies by 0.028% and 0.072%. Overall, we can say that the nearest-neighbor coupling approach has a very slight effect on the results.

[1] P. J. Schmid and D. S. Henningson, *Stability and Transition in Shear Flows*, Applied Mathematical Sciences Vol. 142 (Springer, Berlin, 2001).

[2] W. Tollmien, Über die Entstehung der Turbulenz, *Vorträge aus dem Gebiete der Aerodynamik und verwandter Gebiete* (Springer, Berlin, 1930), pp. 18–21.

[3] L. M. Mack, Boundary-layer linear stability theory, (1984), https://apps.dtic.mil/sti/pdfs/ADA147243.pdf.

[4] S. Chandrasekhar, The character of the equilibrium of an incompressible heavy viscous fluid of variable density, Math. Proc. Camb. Phil. Soc. **51**, 162 (1955).
[5] S. C. Reddy and D. S. Henningson, Energy growth in viscous channel flows, J. Fluid Mech. **252**, 209 (1993).
[6] S. A. Orszag and A. T. Patera, Secondary instability of wall-bounded shear flows, J. Fluid Mech. **128**, 347 (1983).
[7] T. Herbert, Secondary instability of plane shear flows—Theory and application, in *Laminar-Turbulent Transition*, International Union of Theoretical and Applied Mechanics, edited by V. V. Kozlov (Springer, Berlin, 1985), pp. 9–20.
[8] Y. Liu, T. A. Zaki, and P. A. Durbin, Floquet analysis of secondary instability of boundary layers distorted by Klebanoff streaks and Tollmien-Schlichting waves, Phys. Fluids **20**, 124102 (2008).
[9] T. M. Fischer and U. Dallmann, Primary and secondary stability analysis of a three-dimensional boundary-layer flow, Phys. Fluids **3**, 2378 (1991).
[10] G. Bonfigli and M. Kloker, Secondary instability of crossflow vortices: Validation of the stability theory by direct numerical simulation, J. Fluid Mech. **583**, 229 (2007).
[11] F. Picella, J. Robinet, and S. Cherubini, On the influence of the modelling of superhydrophobic surfaces on laminar–turbulent transition, J. Fluid Mech. **901**, A15 (2020).
[12] P. Tabeling, O. Cardoso, and B. Perrin, Chaos in a linear array of vortices, J. Fluid Mech. **213**, 511 (1990).
[13] C.-M. Ho and L.-S. Huang, Subharmonics and vortex merging in mixing layers, J. Fluid Mech. **119**, 443 (1982).
[14] P. J. Schmid, M. F. de Pando, and N. Peake, Stability analysis for n-periodic arrays of fluid systems, Phys. Rev. Fluids **2**, 113902 (2017).
[15] B. J. Olson, S. W. Shaw, C. Shi, C. Pierre, and R. G. Parker, Circulant matrices and their application to vibration analysis, Appl. Mech. Rev. **66**, 040803 (2014).
[16] M. Högberg and D. Henningson, Secondary instability of cross-flow vortices in Falkner–Skan–Cooke boundary layers, J. Fluid Mech. **368**, 339 (1998).
[17] J. Serpieri and M. Kotsonis, Three-dimensional organisation of primary and secondary crossflow instability, J. Fluid Mech. **799**, 200 (2016).
[18] W. Koch, F. P. Bertolotti, A. Stolte, and S. Hein, Nonlinear equilibrium solutions in a three-dimensional boundary layer and their secondary instability, J. Fluid Mech. **406**, 131 (2000).
[19] P. Wassermann and M. Kloker, Mechanisms and passive control of crossflow-vortex-induced transition in a three-dimensional boundary layer, J. Fluid Mech. **456**, 49 (2002).
[20] J.-C. Loiseau, Dynamics and global stability analysis of three-dimensional flows, Ph.D. thesis, Ecole nationale supéérieure d'arts et méétiers, Paris, 2014.
[21] W. D. Heiss, The physics of exceptional points, J. Phys. A: Math. Theor. **45**, 444016 (2012).
[22] L. N. Trefethen, *Spectral Methods in MATLAB*: *Software, Environments and Tools* (Society for Industrial and Applied Mathematics, 2000).
[23] V. M. Falkneb and S. Skan, LXXXV. Solutions of the boundary-layer equations, Lond. Edinb. Dubl. Phil. Mag. J. Sci. **12**, 865 (1931).
[24] J. C. Cooke, The boundary layer of a class of infinite yawed cylinders, Math. Proc. Cambridge Philos. Soc. **46**, 645 (1950).
[25] B. Müller, Experimental study of the travelling waves in a three-dimensional boundary layer, in *Laminar-Turbulent Transition*, edited by D. Arnal and R. Michel (Springer, Berlin, 1990), pp. 489–498.
[26] J. O. Pralits, E. Alinovi, and A. Bottaro, Stability of the flow in a plane microchannel with one or two superhydrophobic walls, Phys. Rev. Fluid **2**, 013901 (2017).
[27] E. B. White and W. S. Saric, Secondary instability of crossflow vortices, J. Fluid Mech. **525**, 275 (2005).
[28] P. Hall, The linear development of Görtler vortices in growing boundary layers, J. Fluid Mech. **130**, 41 (1983).
[29] J. Serpieri, Cross-flow instability, Ph.D. thesis, Delft University of Technology, 2018.
[30] T. Kato, *Perturbation Theory for Linear Operators* (Springer-Verlag, New York, 1995).
[31] M. R. Malik, F. Li, and C.-L. Chang, Crossflow disturbances in three-dimensional boundary layers: Nonlinear development, wave interaction and secondary instability, J. Fluid Mech. **268**, 1 (1994).

[32] S.-T. Wei and C. Pierre, Localization phenomena in mistuned assemblies with cyclic symmetry Part I: Free vibrations, J. Vib. Acoust. Stress Reliability Design **110**, 429 (1988).

[33] S.-T. Wei and C. Pierre, Localization phenomena in mistuned assemblies with cyclic symmetry Part II: Forced vibrations, J. Vib. Acoust. Stress Reliability Design **110**, 439 (1988).

[34] A. Orchini, C. F. Silva, G. A. Mensah, and J. P. Moeck, Thermoacoustic modes of intrinsic and acoustic origin and their interplay with exceptional points, Combust. Flame **211**, 83 (2020).